

See discussions, stats, and author profiles for this publication at: <https://www.researchgate.net/publication/321105532>

# Encapsulation of *E. coli* in biomimetic and Fe<sub>3</sub>O<sub>4</sub> doped hydrogel: Structural and viability analyses

Article in *Applied Microbiology and Biotechnology* · November 2017

DOI: 10.1007/s00253-017-8625-6

CITATIONS

5

READS

108

3 authors:



**Sabella Kiprono**

Masinde Muliro University of Science and Technology

9 PUBLICATIONS 32 CITATIONS

[SEE PROFILE](#)



**Muhammad Wajid Ullah**

Huazhong University of Science and Technology

88 PUBLICATIONS 563 CITATIONS

[SEE PROFILE](#)



**Guang Yang**

Huazhong University of Science and Technology

135 PUBLICATIONS 2,720 CITATIONS

[SEE PROFILE](#)

Some of the authors of this publication are also working on these related projects:



tissue engineering [View project](#)



Scientific research [View project](#)

# Encapsulation of *E. coli* in biomimetic and Fe<sub>3</sub>O<sub>4</sub>-doped hydrogel: structural and viability analyses

Sabella Jelimo Kiprono<sup>1,2,3</sup> · Muhammad Wajid Ullah<sup>1,2</sup> · Guang Yang<sup>1,2</sup> 

Received: 31 July 2017 / Revised: 2 November 2017 / Accepted: 3 November 2017  
© Springer-Verlag GmbH Germany, part of Springer Nature 2017

**Abstract** The current study reports the modification of prokaryotic microorganism through a single-layer technique by using different polyanions/cations and doping with magnetic (Fe<sub>3</sub>O<sub>4</sub>) nanoparticles. Briefly, individual *Escherichia coli* cells were encapsulated through deposition of 1% sodium alginate as first layer followed by depositing precipitate layers of calcium chloride, disodium hydrogen phosphate, and Fe<sub>3</sub>O<sub>4</sub> nanoparticles. Surface and cross sectional analysis of modified *E. coli* cells by field emission scanning electron microscope (FE-SEM) confirmed the synthesis of varying sizes of artificial shells around the microbial cells while the deposition of Fe<sub>3</sub>O<sub>4</sub> nanoparticles was confirmed by transmission electron microscope (TEM). Thermogravimetric analysis (TGA) showed the deposition of 58 wt% of Fe<sub>3</sub>O<sub>4</sub> nanoparticles on *E. coli* cell surface. Chemical structure analysis by Fourier transform infrared (FTIR) spectroscopy confirmed

the presence of characteristic functional groups of deposited reagents in the hydrogel capsule. Zeta potential analysis of hydrogel capsule showed moderate stability with a surface charge of −21 mV. Growth and viability analysis by Alamar Blue assay indicated marked increase in the reduction of resazurin blue (> 100%) by the modified *E. coli* indicating their viability. The movement and control of magnetized *E. coli* cells were manipulated using external permanent magnetic field as observed with optical microscope images. The surface-modified cells can find potential applications in bioremediation, biodegradation, and catalysis and can be used as biosorbents.

**Keywords** Biomimetic modification · Microorganisms · Encapsulation · Nanoparticles · Cell viability

## Introduction

Different living organisms including mollusks, arthropods, radiolarians, diatoms, and fungi protect their species under unfavorable conditions by preserving their genetic materials within a hard shell. Unfortunately, a number of these unicellular organisms in nature do not possess such structured shells to give enough protection to their genetic contents, hence are at risk of extinction. To date, several strategies such as layer-by-layer (LbL) and adsorption (Nguyen et al. 2015), direct single-step magnetization (García-alonso et al. 2010), and extrusion (Poncelet et al. 2011) have been effectively used for cell surface modification. These strategies involve the use of polyelectrolytes, colloids, and molecules to impart surface modifications onto cell walls or membranes of living cells by creating artificial shells or capsules (Yu and Colfen 2004). Surface modification of living microorganisms through biomimetic mineralization has resulted in generation of living

Sabella Jelimo Kiprono and Muhammad Wajid Ullah contributed equally to this work.

**Electronic supplementary material** The online version of this article (<https://doi.org/10.1007/s00253-017-8625-6>) contains supplementary material, which is available to authorized users.

✉ Guang Yang  
yang\_sunny@yahoo.com

<sup>1</sup> Department of Biomedical Engineering, Huazhong University of Science and Technology, Wuhan 430074, People's Republic of China

<sup>2</sup> National Engineering Research Centre for Nano-Medicine, Huazhong University of Science and Technology, Wuhan 430074, China

<sup>3</sup> Department of Medical Laboratory Sciences, Masinde Muliro University of Science and Technology, Kakamega 190-50100, Kenya

mineral complexes with external shells or internal scaffolds (Chen et al. 2014). Fabrication of biomimetic structures along with living cells encapsulated with artificial shells provides the base for nanotechnology science that cuts across chemistry, biology, and material science (Fakhrullin et al. 2012; Ullah et al. 2017).

Most of prokaryotic and eukaryotic microbial cells are diamagnetic in nature; therefore, magnetic techniques are applied by introducing magnetic nanoparticles (MNPs) (Ul-Islam et al. 2017) into or onto live cells as an effective means for remote magnetic field-based control of spatial deposition of cells and fabrication of layered tissue-like structures (Ito et al. 2004). Microbial cells can be post-magnetized by a non-specific attachment of magnetic nanoparticles or by covalent binding on magnetic support. Such modified cells can then be used as magnetic biosorbents or magnetic whole-cell biocatalysts (Safarik and Safarikova 2007). Furthermore, these modified cells have found different applications like toxicological microscreening (García-Alonso et al. 2011), genotoxicity screening (Fakhrullin et al. 2010a), biodegradation (Li et al. 2013b), bioremediation (Zhang et al. 2011a), adsorption (Zhang et al. 2011b; Li et al. 2013a), and biological storage and protection (Wang et al. 2008).

Biomimetic mineralization process of living cells by using different polyelectrolytes or polymers can be improvised by depositing functional factors onto the cell surface (Soledad Fernandez et al. 2001). The deposition of polyelectrolyte or polymer microcapsules can be carried out using the LbL technique (Sukhorukov et al. 1998). This process involves the deposition of polycation first onto the cell surface (carrying a negative charge in water) followed by a polyanion until the required number of bilayers is obtained (Fakhrullin et al. 2012). Besides, a single-step technique has also been used to deposit functional polymers and magnetic nanoparticles onto the cell surface (Fakhrullin et al. 2010b). Variety of synthetic polycations are involved during LbL process, such as poly(styrene sulfonate) (PSS), poly(allylamine hydrochloride) (PAH) (Granicka et al. 2009), and poly(ethyleneimine) (PEI) (Bieber et al. 2002). Some of these polycations have been identified to have several limitations associated with them; for example, polycations present in polyelectrolytes have shown to be toxic since they penetrate into the cell membrane and kill the cell (Godbey et al. 1998; Bieber et al. 2002). This toxic effect of polycations can be minimized by using natural polymers such as poly(L-lysine) (PLL), polypeptides, and hyaluronic acid (HA) to encapsulate the cells (Veerabadrán et al. 2007). Cell surface modification process is limited not only to microbial cells but also to human cells; for instance, modification of mouse mesenchymal stem cells (MSCs) within polymeric shells consisting of HA and PLL using the LbL technique has been reported (Veerabadrán et al. 2007). The HL60 cells and islets have also been modified by using PSS and PAH nanoparticles (Granicka et al. 2009).

Alginate being a natural polymer has been employed in most biofabrication processes for various biomedical applications owing to its biocompatibility and gel formation ability in the presence of calcium ions (de Lima et al. 2009; Lan et al. 2010; Aljohani et al. 2017a, b). Calcium ions serve as useful cross-linking agents to cross-link alginate and form the hydrogel in dispensing-based biofabrication processes. Encapsulation of living cells, probiotics, and enzymes by alginate hydrogels has been extensively used owing to their simple synthesis methods and structure, biocompatibility, non-toxicity, and low cost (Rowley et al. 1999; Krasaekoopt et al. 2003; Ullah et al. 2014; Ullah et al. 2015). Besides, calcium can cross-link with phosphate and form calcium phosphate hybrid nanoparticles (CaP-HNPs) in aqueous solution through self-assembly. This process involves two oppositely charged polyelectrolytes, poly(diallyldimethylammonium chloride) (PDADMAC) and poly(acrylate sodium) (PAS), which serve as dual templates. The formation of complexes of PAS/Ca<sup>2+</sup> and PDADMAC/PO<sub>4</sub><sup>3-</sup> involves electrostatic interactions of positive and negative charges which assemble and form CaP-HNPs. This complex is spherical in shape, dispersible in water, possesses narrow size distribution, and demonstrates high colloidal stability in water (Zhao et al. 2013), thus can be easily deposited on the cell surface. Recently, Shi et al. developed a strategy to dope microbial cells with Fe<sub>3</sub>O<sub>4</sub> nanoparticles through the formation of sodium alginate gel on the cell surface. The manipulated microbial cells efficiently responded to magnetic stimulus and moved within a magnetic field without any interference and effect on their viability and metabolism (Shi et al. 2016).

Surface modification or biomimetic mineralization has been reported mostly for eukaryotic cells (yeast). The current study is aimed to evaluate the success of single-step biomimetic mineralization and magnetization of prokaryotic cell (e.g., *Escherichia coli*) by using different polyanions and cations and doped with magnetic (Fe<sub>3</sub>O<sub>4</sub>) nanoparticles. It describes the biomineralization process of *E. coli*. The surface-modified cells have been characterized for various properties through different techniques such as TEM, SEM, thermogravimetric analysis (TGA), and zeta potential. Further, the viability of encapsulated *E. coli* cells inside the capsule was also evaluated to investigate the toxicity of polycations and anions used. The magnetic properties of the magnetized *E. coli* cells were studied which demonstrated that the magnetically modified *E. coli* cells can assemble in the presence of a permanent magnet. The magnetic-modified *E. coli* cells were viable even after exposure to magnetic fields, hence showing their potential to be used as biosensor and in environmental microbiology such as bioremediation of toxic heavy metals (Pb, Hg) that are risk to human health.

## Materials and methods

### Materials

The chemical reagents including low-molecular-weight sodium alginate ( $C_6H_7NaO_6$ )<sub>n</sub>, anhydrous calcium chloride ( $CaCl_2$ ), disodium hydrogen phosphate dodecahydrate ( $Na_2HPO_4 \cdot 12H_2O$ ), iron (III) chloride hexahydrate ( $FeCl_3 \cdot 6H_2O$ ,  $\geq 98\%$ ), iron (II) chloride tetrahydrate ( $FeCl_2 \cdot 4H_2O$ ,  $\geq 99\%$ ), ammonia solution, phosphotungstic acid, and sodium hydroxide were obtained from Sinopharm Chemical Reagent (Shanghai, China). The nutrient broth for *E. coli* was purchased from Qingdao Hope-Technology Company, China.

### Microorganism and cell culture

*E. coli* (ATCC 11775) cells were obtained from China General Microbiological Culture Collection Center. The *E. coli* cells were grown in nutrient broth of pH 7.0 at 37 °C for 24 h. The freshly prepared cultures were centrifuged at 7000 rpm for 10 min and the pellets obtained were washed three times with distilled water to remove any medium components.

### Synthesis and characterization of $Fe_3O_4$ nanoparticles

The magnetic nanoparticles were synthesized from an aqueous solution of  $FeCl_3 \cdot 6H_2O$  and  $FeCl_2 \cdot 4H_2O$  using the coprecipitation method (Darwish et al. 2015). Briefly,  $FeCl_2 \cdot 4H_2O$  and  $FeCl_3 \cdot 6H_2O$  at a molar ratio 2:1 ( $Fe^{3+}/Fe^{2+}$ ) were dissolved in deionized distilled water and heated at 70 °C. Thereafter, 6 mL of ammonium solution was quickly added to the reaction mixture that resulted in the formation of a deep black magnetite precipitate. The obtained suspension was stirred at 70 °C for 30 min. The obtained precipitate was washed several times with distilled water and extracted from the impurities (if any) using a permanent magnet and washed again until the pH of the supernatant reached 7.0. The obtained nanoparticles were oven-dried at 70 °C and stored in dark at room temperature for further analysis. The chemical structure and confirmation of synthesized magnetic nanoparticles were done through FTIR using a Perkin Elmer FTIR spectrophotometer (Spectrum GX and Autoimage, USA; spectral range 4000–400  $cm^{-1}$ ; beam splitter: Ge-coated on KBr; detector: DTGS; resolution 0.25  $cm^{-1}$  (step selectable)). Similarly, the size and morphology of magnetic nanoparticles were determined through TEM. For this purpose, magnetic nanoparticles were coated onto the carbon coated formvar film and stained with 1% (w/v) phosphotungstic acid (pH 7.0) for few minutes and examined through TEM.

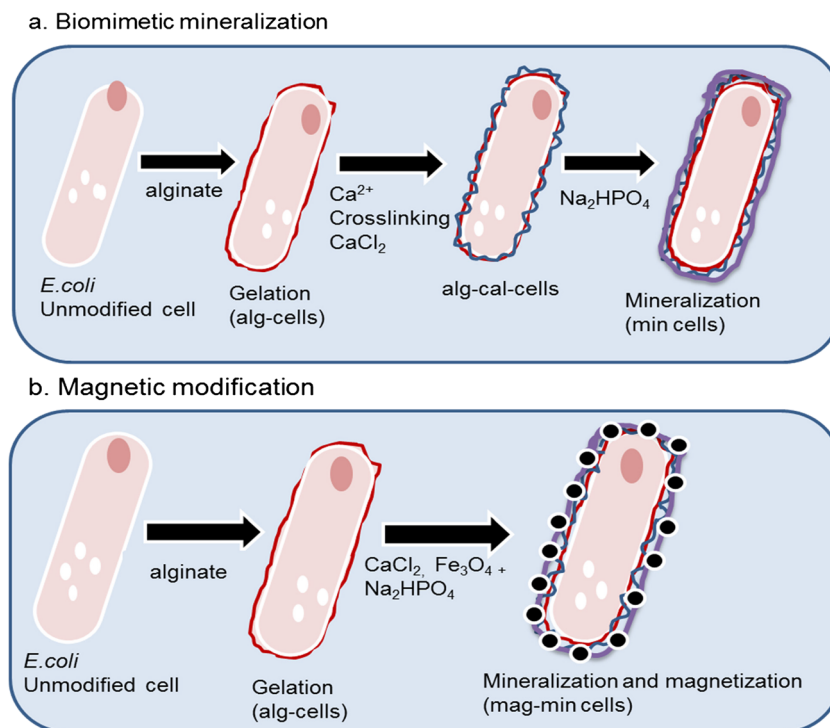
### Biomimetic mineralization and $Fe_3O_4$ doping of *E. coli* cell surface

The synthesized magnetic nanoparticles were suspended in distilled water (0.05 wt%) by vortexing. The magnetic nanoparticles were added to a mixture of 0.005 M aqueous  $CaCl_2$  and 0.005 M  $Na_2HPO_4$  and sonicated for 10 min to stabilize the synthesized magnetite with the precipitate. The mixture was isolated using a permanent magnet and washed again with distilled water and sonicated. On the other hand, *E. coli* cells were harvested from an overnight culture via centrifugation and washed three times with distilled water. A detailed biomimetic mineralization and  $Fe_3O_4$  doping of *E. coli* cell surface are shown in Fig. 1. Briefly, the harvested *E. coli* cells were suspended in 0.1% sodium alginate solution and vortexed for 5 min and left to stand for 20 min to form a single alginate layer around the *E. coli* cells. The alginate-coated *E. coli* cells were harvested and washed with sterile distilled water three times to remove excess alginate and named as “alg-cells.” Thereafter, 1 ml of alg-cells was mixed with 10 ml of precipitate mixture of stabilized  $CaCl_2$ ,  $Fe_3O_4$ , and  $Na_2HPO_4$  ( $CaHPO_4$ - $Fe_3O_4$  stabilized complex) and vortexed for 15 min. The modified *E. coli* cells were separated from the unbound magnetic nanoparticles using a permanent magnet and washed several times with distilled water. These modified *E. coli* cells were named as “mag-min-cells.” A 0.1% sodium alginate solution was added to the cells, vortexed for 5 min, and left to stand for 20 min followed by washing and suspending in 0.005 M aqueous  $CaCl_2$  and finally in 0.005 M  $Na_2HPO_4$  solution. The mineralized cells were left to stand for 20 min to form a precipitate layer on the surface of alginate-coated cells. The coated cells were washed with distilled sterile water and named “min-cells.” Cells modified with single layer of alginate followed by suspension in single layer of calcium chloride were named “Ca-alg-cells.” Finally, all the modified cells were fixed with 3% glutaraldehyde and dehydrated with different dilutions of ethanol (30, 50, 70, 90, and 100%).

### FE-SEM analysis of unmodified and surface-modified *E. coli* cells

The surface of unmodified *E. coli* cell, alg-cells, and min-cells was all analyzed through FE-SEM (Nova NanoSEM450, FEI, Holand). Briefly, alg-cells and min-cells were fixed with 3.0% (v/v) glutaraldehyde in 0.2 M phosphate buffer for 1.0 h at 4 °C. Thereafter, the cells were washed with 0.1 M phosphate buffer at pH 7.0 and dehydrated with different dilutions of ethanol (30, 50, 70, 90, and 100%). The modified cells were freeze-dried and sputter-coated with a thin copper film and placed on the grid followed by gold coating and observed under scanning electron microscope. The unmodified *E. coli* cells were used as reference.

**Fig. 1** Single-step process of biomimetic mineralization (a) and magnetic modification (b) of *E. coli* cells with different polyanions and cations. The *E. coli* cells were modified with single layer of a polyanion alginate (gelation), polycation (calcium chloride and disodium hydrogen phosphate) (mineralization), and  $\text{Fe}_3\text{O}_4$  nanoparticles (magnetization)



### TEM analysis of unmodified and surface-modified *E. coli* cells

The surface and cross section of unmodified *E. coli* cell, alg-cells, min-cells, and mag-min-cells were observed through TEM. Briefly, the glutaraldehyde-fixed cells were embedded in 2.25% (w/v) low-gelling-temperature agarose. Thereafter, the agarose blocks were dehydrated by using different dilutions of ethanol (25, 50, 70, 95, and 100%) for 15 min followed by dehydration in propylene oxide. After an overnight infiltration in Epon 812-propylene oxide (1:1), the agarose blocks were embedded in fresh resin and polymerized. Ultrathin sections ( $80 \pm 20$  nm) were cut using an ultramicrotome EM UC7 (Leica, Germany) and stained with uranyl acetate and lead citrate. Finally, the modified cells were observed using TEM (Hitachi H-7000FA, Japan) operated at 75 kV. Here, the unmodified *E. coli* cells were used as reference.

### TGA analysis of surface-modified *E. coli* cells

TGA was performed to determine the percentage of magnetic nanoparticles present in the sample by using a thermogravimetric analyzer (NETZSCH STA 449F3, Japan). Briefly, a sample of 5 mg was weighed and heated at a rate of  $10^\circ\text{C}/\text{min}$  under nitrogen at temperature range of  $50\text{--}700^\circ\text{C}$ . The iron oxide content in the sample was calculated based on the formula below. Mass of the residue is mass

of the sample remained at  $700^\circ\text{C}$ . Origin 8 software was used to draw the graphs.

$$\text{Iron oxide composition (wt\%)} = \frac{\text{Mass of the residue}}{\text{Mass of the dried sample}} \times 100$$

### FTIR analysis of unmodified and surface-modified *E. coli* cells

FTIR analysis was carried out for five groups of samples including (a) unmodified *E. coli* cell, (b) alg-cells, (c) Ca-alg-cells, (d) min-cells, and (e) mag-min-cells. FTIR was done using a Perkin Elmer FTIR spectrophotometer (Spectrum GX and Autoimage, USA; spectral range  $4000\text{--}400\text{ cm}^{-1}$ ; beam splitter: Ge-coated on KBr; detector: DTGS; resolution  $0.25\text{ cm}^{-1}$  (step selectable)) for identification of chemical bonds and possible interactions between the components in the modified cells. Graphical analysis was done by Origin 8 software.

### Zeta potential analysis of unmodified and surface-modified *E. coli* cells

Zeta potential was performed for five groups of samples including (a) unmodified *E. coli* cell, (b) alg-cells, (c) Ca-alg-cells, (d) min-cells, and (e) mag-min-cells. A Zetasizer Nano machine (Nano-ZS90) was used to determine the surface charge of the coated cells and colloidal stability of artificial shell formed

around the cell. For charge determination, the samples were placed in a zeta cell and loaded into the Nano-Zetasizer machine. All measurements were taken at pH between 7 and 8.

### Alamar Blue assay of unmodified and surface-modified *E. coli* cells

The viability of modified cells was determined through Alamar Blue staining. Briefly, a 100  $\mu\text{l}$  of each (a) unmodified *E. coli* cell, (b) alg-cells, (c) Ca-alg-cells, (d) min-cells, and (e) mag-min-cells and nutrient broth (blank or negative control) were plated into the 96-well plates and mixed well. A 10  $\mu\text{l}$  of the Alamar Blue dye was added to each well containing 100  $\mu\text{l}$  of the cells. The modified *E. coli* cells with the dye were incubated at 37 °C for 4 h. As a result of incubation with viable cells, the dye changed color from blue to red. The absorbance of Alamar Blue dye was measured at 570 nm using 600 nm as a reference. The analysis was done in triplicate by using a plate reader. One-way ANOVA was done by using Origin 8 data analysis graphic software.

### Magnetic properties and viability of magnetic-modified *E. coli* cells

To test the magnetic properties of the cells, mag-min-cells were observed using an optical microscope (Nikon-Ti 80, Japan). A magnet was placed on the sides of the slide containing magnetic-modified *E. coli* cells. The LIVE/DEAD Cell Vitality Assay was performed for the cells after exposure to magnetic field. The kit has two-color fluorescence assay that distinguishes metabolically active cells from injured cells and dead cells. This assay is based on the reduction of  $C_{12}$ -resazurin to red-fluorescent C-resorufin in metabolically active cells and the uptake of cell impermeant, green-fluorescent nucleic acid stain, and SYTOX Green dye, in cells with compromised plasma membranes (usually late apoptotic and necrotic cells). Dead cells emit mostly green fluorescence whereas the healthy and metabolically active cells emit mostly red fluorescence because they possess intact membranes. Briefly, 1  $\mu\text{l}$  of each 50  $\mu\text{M}$   $C_{12}$ -resazurin and SYTOX Green stains were added to 100  $\mu\text{l}$  of cell suspension. The cells were incubated at 37 °C for 15 min; following which, these were immediately observed under the optical microscope (Nikon-Ti 80 Japan) equipped with objective lenses with integrated digital camera and imaging software.

## Results

### Synthesis and characterization of $\text{Fe}_3\text{O}_4$ nanoparticles

The synthesis and chemical structure of  $\text{Fe}_3\text{O}_4$  nanoparticles were confirmed through TEM and FTIR, respectively. The

TEM image shown in Fig. 2a indicates successful synthesis of spherical  $\text{Fe}_3\text{O}_4$  nanoparticles. It was also evident that the particles were agglomerated. Magnetite nanoparticles have high surface energy and thus tend to quickly aggregate; therefore, the agglomeration is prevented by coating them with an organic or inorganic layer (Cao et al. 2012a, b). The particle size and relative particle size distribution was determined through Image J software using the TEM image (Fig. 2a). The results indicated that most of the nanoparticles were in the range of 9–22 nm, with an average particle size of  $16.2 \pm 5$  nm. These results demonstrate that magnetic nanoparticles have narrow size distribution and uniform spherical shape. The FTIR spectrum of  $\text{Fe}_3\text{O}_4$  nanoparticles (Fig. 2b) showed a clear band at  $3438\text{cm}^{-1}$  indicating the hydroxyl (–OH) group and another band at  $587\text{cm}^{-1}$  which is related to Fe–O group, thus confirmed the phase and purity of magnetite nanoparticles which is in agreement with previous report (Garca Casillas et al. 2012).

### Biomimetic mineralization and $\text{Fe}_3\text{O}_4$ doping of *E. coli* cell surface

The cell surface modification was carried out as described in Fig. 1. TEM analysis of unmodified *E. coli* cell surface demonstrated a smooth appearance (Fig. 3a). In contrast, the surface of alg-cells possessed a thick shell of alginate (Fig. 3b) which is in agreement with optical microscopy analysis. TEM analysis also confirmed the synthesis of calcium phosphate shell by the addition of calcium chloride and sodium hydrogen phosphate to the alg-cells as shown in Fig. 3c (min-cells). It is clearly shown in Fig. 3c that the calcium phosphate shell on the surface of the cell is thin and non-uniform (heterogeneous surface) which is in accordance with previous study (Wang et al., 2008). Finally, the cells were doped with the  $\text{Fe}_3\text{O}_4$  nanoparticles to form mag-min-cells (Fig. 3d). SEM analysis showed a rod-like appearance of unmodified *E. coli* cells (Fig. 3e) and alg-cells (Fig. 3f). Figure 3g shows in situ precipitate surface of calcium hydrogen phosphate shell (min-cells). The magnetic property of mag-min-cells was confirmed by suspending the cells in water and a permanent magnet was applied at different sides. The cells effectively moved towards the magnet leaving behind a clear solution as shown in Fig. 3h.

### Thermogravimetric analysis

The magnetic response of the cells is mainly due to the magnetic nanoparticles content loaded on the cell surface. Therefore, TGA was carried out to determine the iron oxide content in the sample and results are shown Fig. 4. The TGA curve shows three phases of weight loss. The first phase of weight loss at 50–125 °C was attributed to the vaporization of small molecules such as water and low-molecular-weight polymers. The second phase ranging from 125 to 250 °C

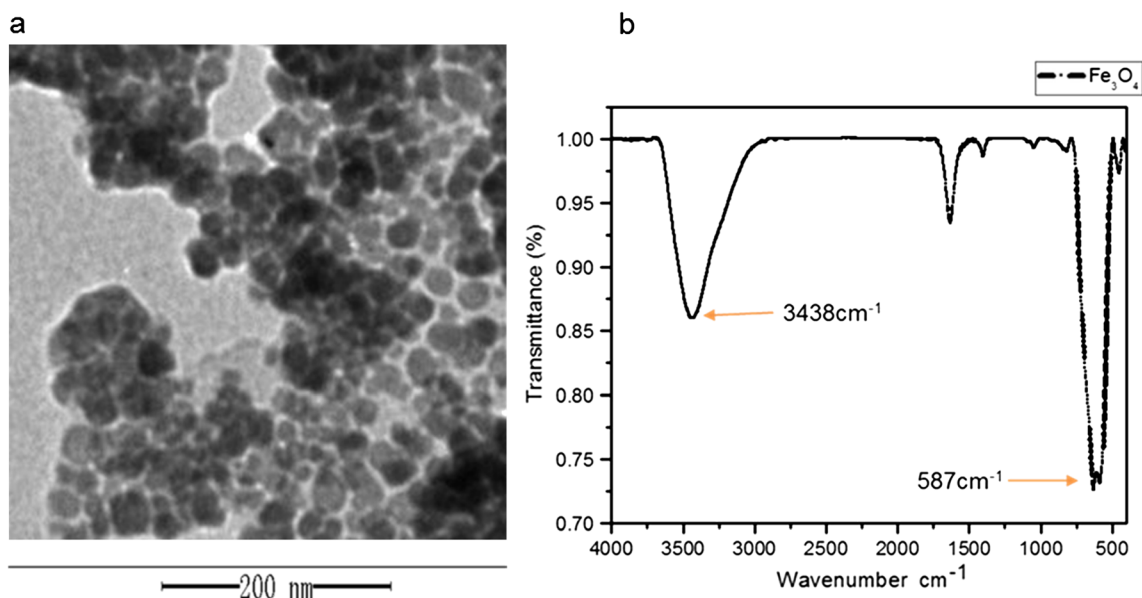


**Fig. 2** **a** TEM micrographs and **b** FTIR spectrum of  $\text{Fe}_3\text{O}_4$  nanoparticles

indicates the decarboxylation of sodium alginate-released carbon dioxide and part of the products were carbonized. The third phase was observed at 250–550 °C indicating the slow decomposition of the higher-molecular-weight species in the sample.

#### FTIR analysis of unmodified and surface-modified *E. coli* cell

FTIR spectroscopy was used to investigate the presence of different functional groups and the nature of chemical bonds in a molecule (Ul-Islam et al. 2011; Ul-Islam et al. 2012). In

the current study, FTIR characterization of five groups of samples including (a) unmodified *E. coli* cell, (b) alg-cells, (c) Ca-alg-cells, (d) min-cells, and (e) mag-min-cells was carried out to identify the presence of different electrolytes and  $\text{Fe}_3\text{O}_4$  nanoparticles on the surface of modified cells and possible interactions between them. The combined spectra for all samples are shown in Fig. 5, indicating the peak positions of various functional groups. Origin 8 software was used to draw the graphs.

FTIR spectra of unmodified *E. coli* cell (Fig. 5a) indicated characteristic peaks at  $3419\text{cm}^{-1}$  for  $-\text{NH}$  groups present on the cell surface. Similarly, the absorption bands at 3395, 3420,

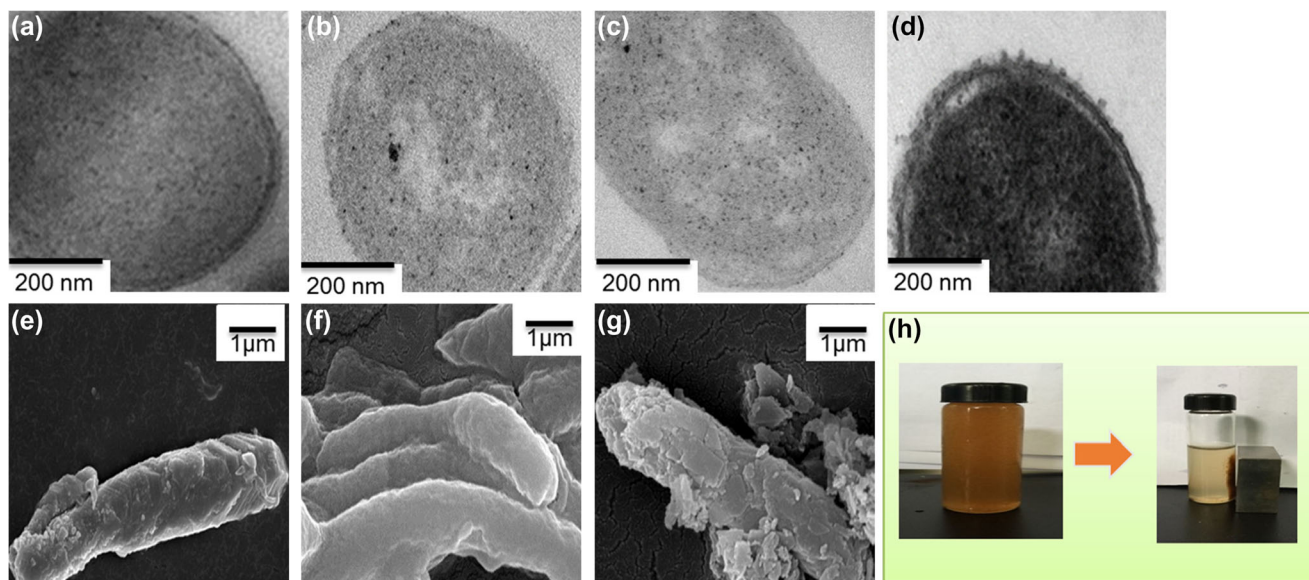


**Fig. 3** Morphological analysis of unmodified and surface-modified *E. coli* cells through various techniques. TEM analysis of **a** unmodified cells, **b** “alg-cells”, **c** “min-cells”, and **d** “mag-min-cells” at 200 nm.

SEM analysis of images of **e** unmodified cell, **f** “alg-cells”, and **g** “min-cells” observed in 1  $\mu\text{m}$  resolution and **h** magnetic property of the modified cells

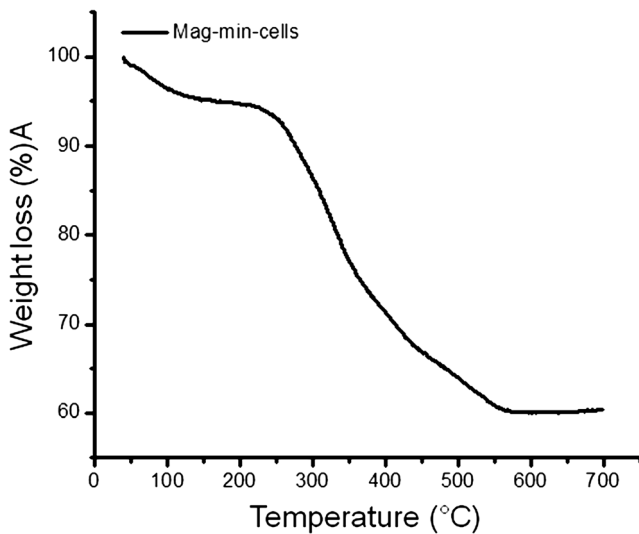


**Fig. 4** Thermogravimetric analysis of magnetic-mineralized *E. coli* cells

3428, and 3408  $\text{cm}^{-1}$  confirmed the stretching vibrations of  $\text{-OH}$  groups on the cell surface. Further, characteristic bands for amide I and amide II groups in bacterial cell wall appeared at 1656  $\text{cm}^{-1}$ . These results were in agreement with previous study (Naumann 2000). The alg-cells (Fig. 5b) showed a lower shift of  $\text{-OH}$  stretching vibration peak at 3395  $\text{cm}^{-1}$  which could be correlated to the interaction of sodium ions with the cell membrane to form a gelation surface (Malesu et al. 2011). When calcium chloride was added to the alg-cells to form the Ca-alg-cells, a shift to a higher wavelength of 3420  $\text{cm}^{-1}$  was observed (Fig. 5c) which could be attributed to the participation of hydroxyl and carboxylate groups of alginate and calcium ion in order to form chelating structure, thus strengthening the hydrogen bonding (Daemi and Barikani 2012).

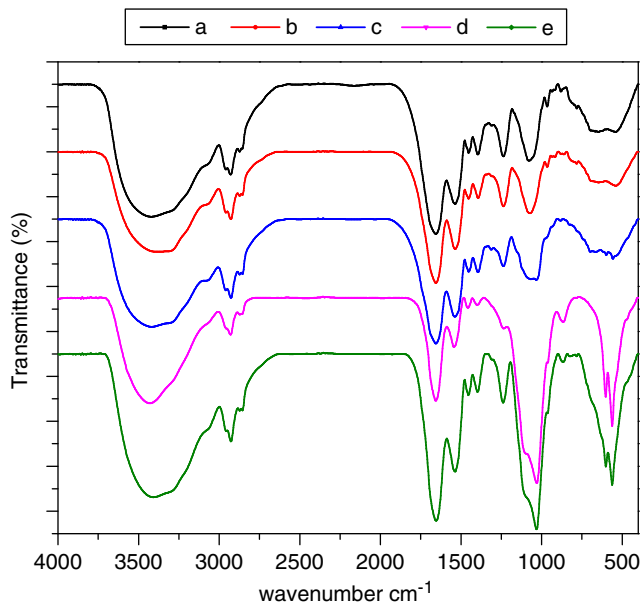


**Fig. 5** FTIR analysis of (a) unmodified cells, (b) “alg-cells”, (c) “Ca-alg-cells”, (d) “min-cells”, and (e) “mag-min-cells”

Further, characteristic peaks at 1029 and 1030  $\text{cm}^{-1}$  for min-cells (Fig. 5d) confirmed the phosphate group single bond which can be attributed to the symmetric stretching mode of non-bridging oxygen in  $\text{Q}^0$  tetrahedral and asymmetric stretching vibration of P-O-P chemical group (Shih 2003; Carta et al. 2007). FTIR spectrum of mag-min-cells (Fig. 5e) showed additional peaks at 561  $\text{cm}^{-1}$  confirming the presence of Fe-O bond and successful attachment of  $\text{Fe}_3\text{O}_4$  nanoparticles. The shift of Fe-O bond to a lower wavelength instead of 587  $\text{cm}^{-1}$  could be due to asymmetrical stretching vibration of Fe-O bond that becomes weak and also due to bending vibration mode of O-P-O chemical group (Elbatal et al. 2011). Generally, the  $\text{PO}_4$  units have two non-bridging bonds and two bridging oxygen bonds (P-O- and P = O) which are in resonance with each other (Bridge and Patel 1987). Besides, peaks appeared at 2927, 2928, 2928, and 2925  $\text{cm}^{-1}$  in samples (b) alg-cells, (c) Ca-alg-cells, (d) min-cells, and (e) mag-min-cells, respectively, for the  $\text{CH}_2$  group of sodium alginate (Zhang et al. 2008). A similar peak in this range at 2928  $\text{cm}^{-1}$  in Fig. 5a appeared for amide I  $\alpha$  helical structure of protein on *E. coli* cell surface (Naumann 2000). Characteristic peak for C = O group appeared at 1655  $\text{cm}^{-1}$  in FTIR spectra of sample (b) alg-cells, (c) Ca-alg-cells, and (d) min-cells, while it appeared at 1654  $\text{cm}^{-1}$  in mag-min-cells which is in accordance with previous study (Malesu et al. 2011).

#### Zeta potential analysis of unmodified and surface-modified *E. coli* cells

Zeta potential is an analytical technique used to investigate the cellular interaction with charged ions or molecules. In principle, the negatively charged ions or molecules decrease the surface zeta potential while positively charged ions increase the surface zeta potential (Altankov et al. 2003). Zeta potential is usually known to determine the colloid stability and some values of zeta potential have been classified to show the stability of a sample. For instance, zeta potential values of samples in range of  $\pm 0$ –10 mV are referred as highly unstable,  $\pm 10$ –20 mV are relatively stable,  $\pm 20$ –30 mV as moderately stable, and  $> \pm 30$  mV are classified as highly stable (Agrawal and Patel 2011). In the current study, zeta potential was performed for five groups of samples including (a) unmodified *E. coli* cell, (b) alg-cells, (c) Ca-alg-cells, (d) min-cells, and (e) mag-min-cells to determine the surface charge of the coated cells and stability of the magnetic mineralized *E. coli* cells. The results are shown in Fig. 6.

As expected, the zeta potential of unmodified *E. coli* cells (Fig. 6a) was found to be  $-51.6$  mV due to the negatively charged cell surface. Upon the addition of sodium alginate, the zeta potential of alg-cells (Fig. 6b) was significantly increased to  $-39$  mV. Further, the addition of calcium chloride Ca-alg-cells (Fig. 6c) shifted the zeta potential value to  $-24.3$  mV which can be attributed to the aggregated alginate

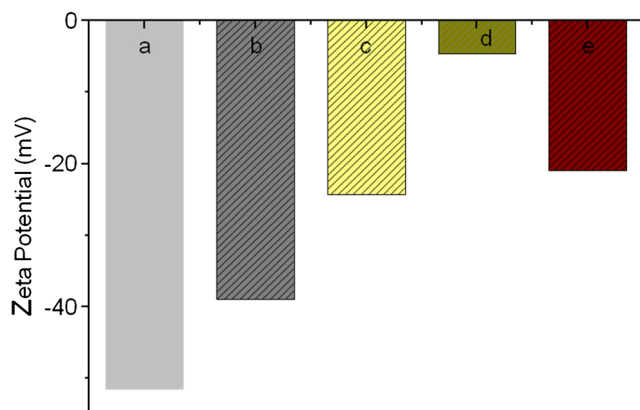


**Fig. 6** Zeta potential analysis of (a) unmodified cells, (b) "alg-cells", (c) "Ca-alg-cells", (d) "min-cells", and (e) "mag-min-cells"

molecules on the cell surface. Studies have shown that  $\text{Ca}^{2+}$  ions selectively bind with guluronic acid (G) residues of alginate and form a cross-link between alginate molecules to form the gel aggregates (Draget et al. 2005). The addition of disodium hydrogen phosphate to the calcium alginate layer on the cell surface resulted in the shift of zeta potential to  $-4.64$  mV (Fig. 6d) which can be attributed to the presence of ions in the higher valency. Usually, the presences of positive charges on the cell surface destabilize the hydrogel. Further, the valency of the ions is also important when measuring the zeta potential. For instance, the ions with higher valency ( $\text{Ca}^{2+}$ ,  $\text{Al}^{3+}$ ) compared to monovalent ions ( $\text{Na}^+$ ,  $\text{H}^+$ , and  $\text{OH}^-$ , etc.) create a more compressed electric double layer on the surface of the particles, therefore decreasing zeta potential in magnitude (Bhattacharjee 2016). A zeta potential of  $-21.0$  mV was observed when  $\text{Fe}_3\text{O}_4$  nanoparticles were loaded on to the precipitate layer of calcium hydrogen phosphate (Fig. 6e). This can be attributed to the negative charge of magnetic nanoparticles that moderately stabilized the hydrogel.

#### Growth and viability analyses of unmodified and surface-modified *E. coli* cells

Alamar Blue assay is based on the principle of reducing resazurin blue dye into a colorless hydroresorufin molecule through an oxygen-consuming metabolic pathway during cell respiration (O'Brian et al. 2000). During this process, viable cells maintain a reducing environment within their cytoplasm. The Alamar Blue reagent is non-fluorescent and blue in color in its oxidized form which turns to fluorescent and red in reduced form upon incubation with viable cells (O'Brian et al. 2000). This indicates that the Alamar Blue reduction is directly related with the cell growth. In the current study, Alamar Blue assay was performed for five groups of samples including (a) unmodified *E. coli* cell, (b) alg-cells, (c) Ca-alg-cells, (d) min-cells, and (e) mag-min-cells to determine the effect of encapsulation, mineralization, and magnetic modification on viability of *E. coli*

cells. The viability results of cells under different encapsulating conditions are summarized in Fig. 7.

As shown in Fig. 7, the unmodified cells were marked by the highest percentage reduction of resazurin blue of about 140% translating to more viable cells as compared to the modified cells (Fig. 7a). The alg-cells also demonstrated a higher percentage of viable cells indicating that sodium alginate is non-toxic to the microbial cell and can effectively support the growth of the cells (Fig. 7b). Cross-linking of alginate modified cells with calcium chloride Ca-alg-cells to form a gelatinous hydrogel could have some impact on the cell growth owing to increased viscosity and mechanical forces (Cao et al. 2012a) as shown in Fig. 7c. Further, the precipitate layer of calcium hydrogen phosphate could be too dense and less porous for the movement of substances inside the cell, thus presented a lower reduction of resazurin blue corresponding to lower number of cells viable inside the mineral shell (Fig. 7d). When the mineral layer was further doped with  $\text{Fe}_3\text{O}_4$  nanoparticles, the surface became more rough and porous and increased the porosity of mineral shell, thus allowing the diffusion of more nutrients to sustain the cell inside the shell as shown by the marked increase in the reduction of resazurin blue (Fig. 7e), corresponding to increasing the number of viable cells.

#### Magnetic properties of surface-modified *E. coli* cell

Surface modification of microbial cells through encapsulation and doping with magnetic nanoparticles enhance the cell's ability to acquire magnetic properties similar to magnetotactic

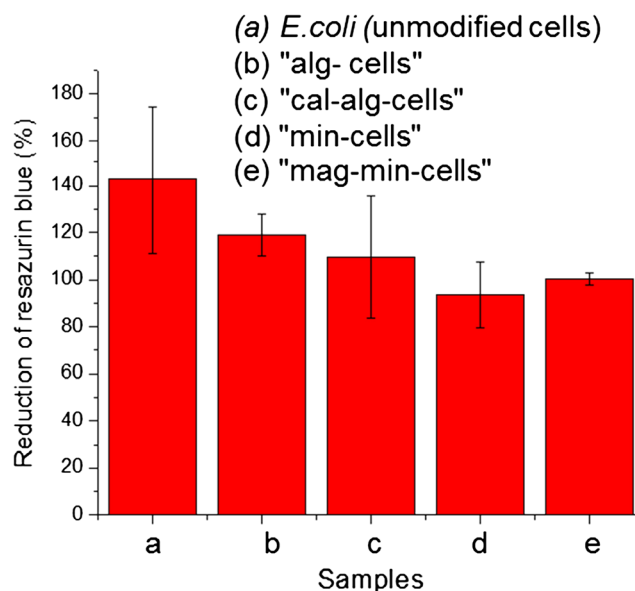


**Fig. 7** Effect of cell surface modification on viability and growth analysis of *E. coli*. The reduction of resazurin blue as a function of viability and growth of (a) unmodified cells, (b) "alg-cells", (c) "Ca-alg-cells", (d) "min-cells", and (e) "mag-min-cells" was determined using Alamar Blue assay

bacteria (Yan et al. 2012). Such magnetically modified cells allow for magnetically facilitated spatial manipulation (Safarik and Safarikova 2007; Safarik et al. 2012). A study reported that magnetophoresis and magnetic alignment of modified yeast cell (@MSi[n]) were due to net magnetization of yeast with magnetic materials @MSi[n] on the cell surface. All magnetized cells were able to be separated and spatially manipulated independently from one another by modulating the external magnetic field. The spatial-temporal control exhibited by yeast @MSi[n] enhanced its application in protein size marker for electrophoresis for guiding samples (Lee et al. 2016). These results were in accordance with our results where the mag-min-cells were able to move towards the magnet or aggregate together when a magnet was placed on the side of the slide. Figure 8a shows that the magnetized cells are scarcely distributed in the absence of any magnetic field to cause their aggregation. In contrast, when a permanent magnet was placed beside the slide, the cells aggregated by moving towards each other (Fig. 8b). These observations were also demonstrated in the video provided in supplementary data (Video S1). The cells were able to move in the presence of a magnet.

Resazurin assay showed that the mag-min-cells were metabolically active even after when mag-min-cells were exposed to magnetic fields for a short period of time. Figure 8c shows the red fluorescence emitted by the live and metabolically active magnetic-modified cells. A biochemical resazurin assay carried out by Konnova et al. showed that the metabolic activity of PAH-MNPs-coated bacteria was partially reduced at higher concentration of magnetic nanoparticles and there was no significant reduction of metabolic activity even at lower concentration of magnetic nanoparticles indicating that the cells were able to retain their normal growth and behavior even in the presence of magnetic nanoparticles and exposure to magnetic fields (Konnova et al. 2016). These results are in agreement with our observations.

## Discussion

In the attempt to modify the cell surface by biomimetic mineralization and doping it with magnetic nanoparticles, it was confirmed that the cells were successfully fabricated with different polycation and anions used. The alg-cells demonstrated a gel-like appearance due to the viscous nature of sodium alginate (Cao et al. 2012a) (Fig. 3b). Cross-linking of alg-cells with  $\text{Ca}^{2+}$  and disodium hydrogen phosphate (Fig. 3c) formed a compatible hydrogel (Cao et al. 2012b; Ullah et al. 2014; Ullah et al. 2015). Doping the calcium phosphate shell with  $\text{Fe}_3\text{O}_4$  nanoparticles resulted in the formation of a rough surface (mag-min-cells) (Fig. 3d), thus confirming the successful fabrication of mag-min-cells. It was also evident that the nanoparticles did not aggregate; rather, these were uniformly distributed on the surface of mineralized cell. Further, SEM results confirmed the fabrication of alg-cells which showed a smooth gel-like structure (Fig. 3f). The min-cells (Fig. 3g) formed a precipitate when combined together to form a rough shell on the surface of the cell (Wang et al. 2008). Figure 3h confirmed the magnetic property of magnetic-modified cells mag-min-cells. The cells remained intact even after removal of magnet (placed beside the vial) for a couple of minutes until they were disassembled through shaking. These results showed that *E. coli* cells were effectively fabricated by different polyanions/cations and successfully magnetized and can be easily manipulated and moved in different directions and positions through the induction of external magnetic field.

The percentage weight of iron oxide content in the sample is shown by TGA curve (Fig. 4). The mass change in the curve between 550 and 700 °C could be attributed to the organic species in the magnetic composite nanoparticles, indicating complete decomposition and that  $\text{Fe}_3\text{O}_4$  nanoparticles remain (Pimpha et al. 2012; Li et al. 2017). The percentage of iron oxide doped onto the cell surface

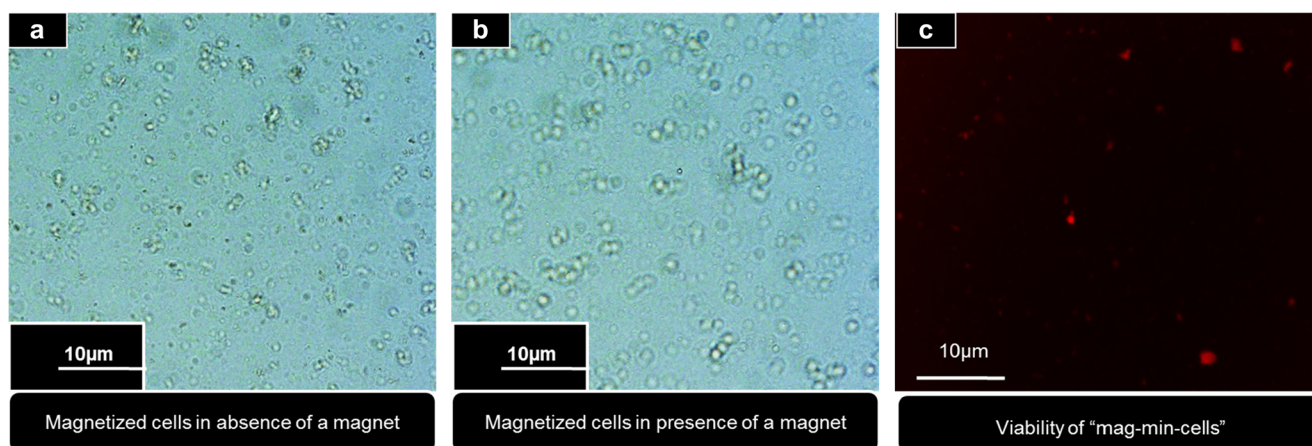


**Fig. 8** Optical images of “mag-min-cells” in the **a** absence and **b** presence of a magnetic field and **c** viability of “mag-min-cells” after exposure to magnetic field

was calculated to be 58 wt% and it was the main contributing factor causing the movement of the cells within a magnetic field. The chemical interaction and bonding among different polyanions/cations and magnetic nanoparticles analyzed by FTIR revealed no significant interference during deposition of the layers. Overall, FTIR spectra of all samples did not show much interference in the bond structure of the hydrogel. The surface charge of unmodified *E. coli* cell was stabilized by fabricating the cells. The polyanions and cations used to coat the *E. coli* cell surface have almost the same functional groups which make the hydrogel stable. Zeta potential revealed that the artificial shell has different colloidal stability (surface charge) depending on the cation and anion used to form the layer. Magnetic-modified *E. coli* cells acquired an outer shell (artificial shell) with a moderate colloidal stability (surface charge of  $-21$  Mv).

The cell growth and viability were not altered by the natural polyanions/cations and magnetic nanoparticles. Modified *E. coli* cells were able to survive and grow inside the shell; thus, the artificial shell offered protection to the *E. coli* cells. The coating materials used to encapsulate the cells were suitable since there was no significant difference in the growth of the cells. The polyelectrolytes and  $\text{Fe}_3\text{O}_4$  nanoparticles were shown to be non-toxic towards the magnetic-modified *E. coli* cells and effectively supported the growth of *E. coli* cells. When cells are alive, they maintain a reducing environment within their cytosol. This indicates that the aerobic respiration of bacteria is not in any way interfered by encapsulation process (O'Brian et al. 2000). Manipulation of cells with magnetic fields did not affect the viability of the cells since most of the cells were able to reduce  $\text{C}_{12}$ -resazurin to red-fluorescent  $\text{C}$ -resorufin (Fig. 8c). The movement of magnetized *E. coli* cells within the magnetic fields was observed; thus, the magnetic-modified *E. coli* cells were easily susceptible for spatial manipulation with a permanent magnet. The spatial movement of magnetically modified *E. coli* cells is attributed to the presence of magnetic nanoparticles on the surface of magnetic-modified *E. coli* cells. The advantage of addition of magnetic functionality to cells allows for effective spatial manipulation using relatively simple and accessible magnetic fields, which dramatically improves the control over geometry, size distribution, and cell distribution (Dzamukova et al. 2015). The current study demonstrated a novel biofabrication strategy for magnetic modification of prokaryotic microorganisms by doping their surfaces with nanoparticles in the presence of single layer of various polyanions/cations. The magnetic fabrication of cells to obtain magnetic property enhances the functionality of the cell to find potential applications in detecting toxic compounds in environment and other biotechnological applications.

**Funding information** This work was supported by National Natural Science Foundation of China (21574050, 21774039, 51603079), China Postdoctoral Science Foundation (2016M602291), Fundamental Research Funds for the Central Universities, and Open Research Fund of State Key Laboratory of Polymer Physics and Chemistry, Changchun Institute of Applied Chemistry, Chinese Academy of Sciences.

**Compliance with ethical standards** This article does not contain any studies with human participants or animals performed by any of the authors.

**Conflict of interest statement** The authors declare that they have no conflict of interest.

## References

- Agrawal Y, Patel V (2011) Nanosuspension: an approach to enhance solubility of drugs. *J Adv Pharm Technol Res* 2(2):81–87. <https://doi.org/10.4103/2231-4040.82950>
- Aljohani WJ, Wenchao L, Ullah MW, Zhang X, Yang G (2017a) Application of sodium alginate hydrogel. *IOSR J Biotechnol Biochem* 03(3):19–31. <https://doi.org/10.9790/264X-03031931>
- Aljohani W, Ullah MW, Zhang X, Yang G (2017b) Bioprinting and its applications in tissue engineering and regenerative medicine. *Int J Biol Macromol*. <https://doi.org/10.1016/J.IJBIOMAC.2017.08.171>
- Altankov G, Richau K, Groth T (2003) The role of surface zeta potential and substratum chemistry for regulation of dermal fibroblasts interaction. *Mater Sci Eng Technol* 34:1120–1128
- Bhattacharjee S (2016) Review article DLS and zeta potential—what they are and what they are not? *J Control Release* 235:337–351. <https://doi.org/10.1016/j.jconrel.2016.06.017>
- Bieber T, Meissner W, Kostin S, Niemann A, Elsasser HP (2002) Intracellular route and transcriptional competence of polyethylenimine-DNA complexes. *J Control Release* 82(2-3):441–454. [https://doi.org/10.1016/S0168-3659\(02\)00129-3](https://doi.org/10.1016/S0168-3659(02)00129-3)
- Bridge B, Patel ND (1987) Composition dependence of the infrared absorption spectra of molybdenum phosphate glasses and some crystalline analogues. *J Non-Cryst Solids* 91(1):27–42. [https://doi.org/10.1016/S0022-3093\(87\)80083-2](https://doi.org/10.1016/S0022-3093(87)80083-2)
- Cao N, Chen XB, Schreyer DJ (2012a) Influence of calcium ions on cell survival and proliferation in the context of an alginate hydrogel. *ISRN Chem Eng* 2012:1–9. <https://doi.org/10.5402/2012/516461>
- Cao X, Zhang B, Zhao F, Feng L (2012b) Synthesis and properties of MPEG-coated superparamagnetic magnetite nanoparticles. *J Nanomater* 2012:5137–5149. <https://doi.org/10.1155/2012/607296>
- Carta D, Pickup DM, Knowles JC, Ahmed I, Smith ME, Newport RJ (2007) A structural study of sol-gel and melt-quenched phosphate-based glasses. *J Non-Cryst Solids* 353(18-21):1759–1765. <https://doi.org/10.1016/j.jnoncrysol.2007.02.008>
- Chen W, Wang G, Tang R (2014) Nanomodification of living organisms by biomimetic mineralization. *Nano Res* 7(10):1404–1428. <https://doi.org/10.1007/s12274-014-0509-9>
- Daemi H, Barikani M (2012) Synthesis and characterization of calcium alginate nanoparticles, sodium homopolymannuronate salt and its calcium nanoparticles. *Sci Iran* 19(6):2023–2028. <https://doi.org/10.1016/j.scient.2012.10.005>
- Darwish MSA, Nguyen NHA, AŞ R, Stibor I (2015) Functionalized magnetic nanoparticles and their effect on *Escherichia coli* and *Staphylococcus aureus*. *J Nanomater* 2015:10
- de Lima DO, Aimoli CG, Beppu MM (2009) Investigation on the biomimetic influence of biopolymers on calcium phosphate precipitation—part 1: alginate. *Mater Sci Eng C* 29(4):1109–1113. <https://doi.org/10.1016/j.msec.2008.09.019>

- Draget KI, Smidsrød O, Skjåk-Bræk G (2005) Alginates from algae. In: Steinbüchel A, Rhee SK (eds) *Polysaccharides and polyamides in the food industry. Properties, production and patents*, 1st edn. Wiley, Germany, pp 1–30
- Dzhamukova MR, Naumenko EA, Rozhina EV, Trifonov AA, Fakhrollin RF (2015) Cell surface engineering with polyelectrolyte-stabilized magnetic nanoparticles: a facile approach for fabrication of artificial multicellular tissue-mimicking clusters. *Nano Res* 8(8):2515–2532. <https://doi.org/10.1007/s12274-015-0759-1>
- Elbatal FH, Marzouk MA, Abdelghany AM (2011) UV-visible and infrared absorption spectra of gamma irradiated V<sub>2</sub>O<sub>5</sub>-doped in sodium phosphate, lead phosphate, zinc phosphate glasses: a comparative study. *J Non-Cryst Solids* 357(3):1027–1036. <https://doi.org/10.1016/j.jnoncrysol.2010.11.040>
- Fakhrollin RF, García-Alonso J, Paunov VN (2010a) A direct technique for preparation of magnetically functionalised living yeast cells. *Soft Matter* 6(2):391–397. <https://doi.org/10.1039/B914065D>
- Fakhrollin RF, Shlykova LV, Zamaleeva AI, Nurgaliev DK, Osin YN, García-Alonso J, Paunov VN (2010b) Interfacing living unicellular algae cells with biocompatible polyelectrolyte-stabilised magnetic nanoparticles. *Macromol Biosci* 10(10):1257–1264. <https://doi.org/10.1002/mabi.201000161>
- Fakhrollin RF, Zamaleeva AI, Minullina RT, Konnova SA, Paunov VN (2012) Cyborg cells: functionalisation of living cells with polymers and nanomaterials. *Chem Soc Rev* 41(11):4189–4206. <https://doi.org/10.1039/c2cs15264a>
- García Casillas PE, Rodríguez González CA, Martínez Prez CA (2012) Infrared spectroscopy of functionalized magnetic nanoparticles. *Infrared Spectrosc Mater Sci Eng Technol*. <https://doi.org/10.5772/35481>
- García-alonso J, Fakhrollin RF, Paunov VN (2010) Rapid and direct magnetization of GFP-reporter yeast for micro-screening systems. *Biosens Bioelectron* 25(7):1816–1819. <https://doi.org/10.1016/j.bios.2009.11.016>
- García-Alonso J, Fakhrollin RF, Paunov VN, Shen Z, Hardege JD, Pamme N, Haswell SJ, Greenway GM (2011) Microscreening toxicity system based on living magnetic yeast and gradient chips. *Anal Bioanal Chem* 400(4):1009–1013. <https://doi.org/10.1007/s00216-010-4241-3>
- Godbey WT, Wu KK, Mikos AG (1998) Size matters : molecular weight affects the efficiency of poly ( ethylenimine ) as a gene delivery vehicle. *J Biomed Mater Res* 45:268–275
- Granicka LH, Antosiak-Iwańska M, Godlewska E, Hoser G, Strawski M, Szklarczyk M, Dudziński K (2009) The experimental study of polyelectrolyte coatings suitability for encapsulation of cells. *Artif Cells Blood Substit Immobil Biotechnol* 37(5):187–194. <https://doi.org/10.1080/10731190903199218>
- Ito A, Takizawa Y, Honda H, Hata K, Kagami H, Ueda M, Kobayashi T (2004) Tissue engineering using magnetite nanoparticles and magnetic force: heterotypic layers of cocultured hepatocytes and endothelial cells. *Tissue Eng* 10(5-6):833–840. <https://doi.org/10.1089/1076327041348301>
- Konnova SA, Lvov YM, Fakhrollin RF (2016) Nanoshell assembly for magnet-responsive oil-degrading bacteria. *Langmuir* 32(47):12552–12558. <https://doi.org/10.1021/acs.langmuir.6b01743>
- Krasaekoopt W, Bhandari B, Deeth H (2003) Evaluation of encapsulation techniques of probiotics for yoghurt. *Int Dairy J* 13(1):3–13. [https://doi.org/10.1016/S0958-6946\(02\)00155-3](https://doi.org/10.1016/S0958-6946(02)00155-3)
- Lan SF, Safiejko-Mroccka B, Starly B (2010) Long-term cultivation of HepG2 liver cells encapsulated in alginate hydrogels: a study of cell viability, morphology and drug metabolism. *Toxicol In Vitro* 24(4):1314–1323. <https://doi.org/10.1016/j.tiv.2010.02.015>
- Lee H, Hong D, Cho H, Kim JY, Park JH, Lee SH, Kim HM, Fakhrollin RF, Choi IS (2016) Turning diamagnetic microbes into multinary micro-magnets: magnetophoresis and spatio-temporal manipulation of individual living cells. *Sci Rep* 6(1):38517. <https://doi.org/10.1038/srep38517>
- Li C, Lu J, Li S, Tong Y, Ye B (2017) Synthesis of magnetic microspheres with sodium alginate and activated carbon for removal of methylene blue. *Materials (Basel)* 10(1):84. <https://doi.org/10.3390/ma10010084>
- Li TT, Liu YG, Peng QQ, Hu XJ, Liao T, Wang H, Lu M (2013a) Removal of lead(II) from aqueous solution with ethylenediamine-modified yeast biomass coated with magnetic chitosan microparticles: kinetic and equilibrium modeling. *Chem Eng J* 214:189–197. <https://doi.org/10.1016/j.cej.2012.10.055>
- Li Y, Du X, Wu C, Liu X, Wang X, Xu P (2013b) An efficient magnetically modified microbial cell biocomposite for carbazole biodegradation. *Nanoscale Res Lett* 8(1):522. <https://doi.org/10.1186/1556-276X-8-522>
- Malesu VK, Sahoo D, Nayak PL (2011) Chitosan–sodium alginate nanocomposites blended with cloisite 30b as a novel drug delivery system for anticancer drug curcumin. *Int J Appl Biol Pharm Technol* 2(1):402–411. <https://doi.org/10.1007/s12588-011-9000-6>
- Naumann D (2000) Infrared spectroscopy in microbiology. In: *Encyclopedia of Analytical Chemistry* pp 1–32
- Nguyen TD, Guyot S, Lherminier J, Wache Y, Saurel R, Husson F (2015) Protection of living yeast cells by micro-organized shells of natural polyelectrolytes. *Process Biochem* 50(10):1528–1536. <https://doi.org/10.1016/j.procbio.2015.06.003>
- O'Brian J, Wilson I, Orton T, Pognan F (2000) Investigation of the Alamar Blue(resazurin) fluorescent dye for the assessment of mammalian cell cytotoxicity. *Eur J Biochem* 267:5421–5426
- Pimpha N, Chaleawler-Umpom S, Sunintaboon P (2012) Core/shell polymethyl methacrylate/polyethyleneimine particles incorporating large amounts of iron oxide nanoparticles prepared by emulsifier-free emulsion polymerization. *Polymer (Guildf)* 53(10):2015–2022. <https://doi.org/10.1016/j.polymer.2012.03.019>
- Poncelet D, Nader-mac EF, Scientific N (2011) Stability of lactobacilli encapsulated in various microbial polymers. *J Biosci Bioeng* 113(2):179–184. <https://doi.org/10.1016/j.jbiosc.2011.10.010>
- Rowley JA, Madlambayan G, Mooney DJ (1999) Alginate hydrogels as synthetic extracellular matrix materials. *Biomaterials* 20(1):45–53. [https://doi.org/10.1016/S0142-9612\(98\)00107-0](https://doi.org/10.1016/S0142-9612(98)00107-0)
- Safarik I, Pospiskova K, Horska K, Safarikova M (2012) Potential of magnetically responsive (nano)biocomposites. *Soft Matter* 8(20):5407. <https://doi.org/10.1039/c2sm06861c>
- Safarik I, Safarikova M (2007) Magnetically modified microbial cells: a new type of magnetic adsorbents. *China Particuology* 5(1-2):19–25. <https://doi.org/10.1016/j.cpart.2006.12.003>
- Shi X, Shi Z, Wang D, Ullah MW, Yang G (2016) Microbial cells with a Fe<sub>3</sub>O<sub>4</sub> doped hydrogel extracellular matrix: manipulation of living cells by magnetic stimulus. *Macromol Biosci* 16(10):1506–1514. <https://doi.org/10.1002/mabi.201600143>
- Shih PY (2003) Properties and FTIR spectra of lead phosphate glasses for nuclear waste immobilization. *Mater Chem Phys* 80(1):299–304. [https://doi.org/10.1016/S0254-0584\(02\)00516-3](https://doi.org/10.1016/S0254-0584(02)00516-3)
- Soledad Fernandez M, Moya A, Lopez L, Arias JL (2001) Secretion pattern, ultrastructural localization and function of extracellular matrix molecules involved in eggshell formation. *Matrix Biol* 19(8):793–803. [https://doi.org/10.1016/S0945-053X\(00\)00128-1](https://doi.org/10.1016/S0945-053X(00)00128-1)
- Sukhorukov GB, Donath E, Lichtenfeld H, Knippel E, Knippel M, Budde A, Möhwald H (1998) Layer-by-layer self assembly of polyelectrolytes on colloidal particles. *Colloids Surf A Physicochem Eng Asp* 137(1-3):253–266. [https://doi.org/10.1016/S0927-7757\(98\)00213-1](https://doi.org/10.1016/S0927-7757(98)00213-1)
- Ul-Islam M, Khan T, Park JK (2012) Nanoreinforced bacterial cellulose-montmorillonite composites for biomedical applications. *Carbohydr Polym* 89(4):1189–1197. <https://doi.org/10.1016/j.carbpol.2012.03.093>

- Ul-Islam M, Shah N, Ha JH, Park JK (2011) Effect of chitosan penetration on physico-chemical and mechanical properties of bacterial cellulose. *Korean J Chem Eng* 28(8):1736–1743. <https://doi.org/10.1007/s11814-011-0042-4>
- Ul-Islam M, Ullah MW, Khan S, Manan S, Khattak WA, Ahmad W, Shah N, Park JK (2017) Current advancements of magnetic nanoparticles in adsorption and degradation of organic pollutants. *Environ Sci Pollut Res* 24(14):12713–12722. <https://doi.org/10.1007/s11356-017-8765-3>
- Ullah MW, Khattak WA, Ul-Islam M, Khan S, Park JK (2014) Bio-ethanol production through simultaneous saccharification and fermentation using an encapsulated reconstituted cell-free enzyme system. *Biochem Eng J* 91:110–119. <https://doi.org/10.1016/j.bej.2014.08.006>
- Ullah MW, Khattak WA, Ul-Islam M, Khan S, Park JK (2015) Encapsulated yeast cell-free system: a strategy for cost-effective and sustainable production of bio-ethanol in consecutive batches. *Biotechnol Bioprocess Eng* 20(3):561–575. <https://doi.org/10.1007/s12257-014-0855-1>
- Ullah MW, Shi Z, Shi X, Di Z, Li S, Yang G (2017) Microbes as structural templates in biofabrication: study of surface chemistry and applications. *ACS Sus Chem Eng*. <https://doi.org/10.1021/acssuschemeng.7b02765>
- Veerabadran NG, Goli PL, Stewart-Clark SS, Lvov YM, Mills DK (2007) Nanoencapsulation of stem cells within polyelectrolyte multilayer shells. *Macromol Biosci* 7(7):877–882. <https://doi.org/10.1002/mabi.200700061>
- Wang B, Liu P, Jiang W, Pan H, Xu X, Tang R (2008) Yeast cells with an artificial mineral shell: protection and modification of living cells by biomimetic mineralization. *Angew Chem Int Ed* 47(19):3560–3564. <https://doi.org/10.1002/anie.200704718>
- Yan L, Zhang S, Chen P, Liu H, Yin H, Li H (2012) Magnetotactic bacteria, magnetosomes and their application. *Microbiol Res* 167(9):507–519. <https://doi.org/10.1016/j.micres.2012.04.002>
- Yu S-H, Colfen H (2004) Bio-inspired crystal morphogenesis by hydrophilic polymers. *J Mater Chem* 14(14):2124–2147. <https://doi.org/10.1039/b401420k>
- Zhang J, Xu S, Zhang S, Du Z (2008) Preparation and characterization of tamarind gum/sodium alginate composite gel beads. *Iran Polym J* 17(12):899–906
- Zhang D, Fakhrollin RF, Özmen M, Wang H, Wang J, Paunov VN, Li G, Huang WE (2011a) Functionalization of whole-cell bacterial reporters with magnetic nanoparticles. *Microb Biotechnol* 4:89–97. <https://doi.org/10.1111/j.1751-7915.2010.00228.x>
- Zhang Y, Zhu J, Zhang L, Zhang Z, Xu M, Zhao M (2011b) Synthesis of EDTAD-modified magnetic baker's yeast biomass for Pb<sup>2+</sup> and Cd<sup>2+</sup> adsorption. *Desalination* 278(1-3):42–49. <https://doi.org/10.1016/j.desal.2011.05.003>
- Zhao XY, Zhu YJ, Chen F, Lu BQ, Qi C, Zhao J, Wu J (2013) Calcium phosphate hybrid nanoparticles: self-assembly formation, characterization, and application as an anticancer drug nanocarrier. *Chem An Asian J* 8(6):1306–1312. <https://doi.org/10.1002/asia.201300083>